Analysis of Phase-Locking in Narrow-Band Optoelectronic Oscillators With Intermediate Frequency

Alain Francis Talla, Romain Martinenghi, Géraud R. Goune Chengui, Jimmi H. Talla Mbé, Khaldoun Saleh, Aurélien Coillet, Guoping Lin, Paul Woafo, and Yanne K. Chembo, *Senior Member, IEEE*

***Abstract*— In this paper, we investigate the phenomenon of phase-locking in laser-based optoelectronic oscillators from the point of view of nonlinear dynamics. We provide a theoretical and experimental analysis of the phase dynamics of these oscillators when driven by an external voltage in the intermediate frequency range. This configuration leads to phase-locking phenomena that can be theoretically analyzed from the viewpoint of Arnold tongues theory. Our research permits to determine analytically the range of parameters where the amplitude and the frequency of the driving source induce phase-locking.**

***Index Terms*— Optoelectronic devices, nonlinear oscillators.**

I. Introduction

OPTOELECTRONIC oscillators (OEOs) are autonomous systems where a signal is alternatively converted into the optical and electrical domains in a closed loop configuration. In general, an optical laser beam is first phase- or amplitude-modulated by a nonlinear element driven by an electric signal. This modulated optical signal is then photodetected, and provides an electrical signal which is eventually amplified and fed back into the light-modulating device [1]–[5].

Manuscript received December 15, 2014; revised February 25, 2015 and April 6, 2015; accepted April 20, 2015. Date of publication April 23, 2015; date of current version May 5, 2015. This work was supported in part by the Centre National d'Etudes Spatiales through the SHYRO Project, in part by the European Research Council through the NextPhase Project and Versyt Project, in part by the Agence Nationale de la Recherché through the ORA Project, in part by the Région de Franche-Comté, and in part by the Labex ACTION. *(Corresponding author: Yanne K. Chembo.)*

A. F. Talla and G. R. Goune Chengui are with the Laboratory of Modeling and Simulation in Engineering, Biomimetics and Prototypes, Department of Physics, University of Yaoundé I, Yaoundé PO Box 812, Cameroon, and also with the African Center of Excellence for Information and Communication Technologies, Polytechnic School of Yaoundé, Yaoundé PO Box 8390, Cameroon (e-mail: frataalai@yahoo.fr; geraud.goune@yahoo.fr).

R. Martinenghi, K. Saleh, G. Lin, and Y. K. Chembo are with the Franche-Comté Électronique Mécanique Thermique et Optique—Sciences et Technologies Institute, Besançon 25030, France (e-mail: romain.martinenghi@femto-st.fr; khaldoun.saleh@femto-st.fr; guoping.lin@femto-st.fr; yanne.chembo@femto-st.fr).

J. H. Talla Mbé and P. Woafo are with the Laboratory of Modeling and Simulation in Engineering, Biomimetics and Prototypes, Department of Physics, University of Yaoundé I, Yaoundé 20521, Cameroon (e-mail: jhtallam@yahoo.fr; pwoafo1@yahoo.fr).

A. Coillet is with the National Institute of Standards and Technology, Boulder, CO 80305 USA (e-mail: acoillet@gmail.com).

Color versions of one or more of the figures in this paper are available online at http://ieeexplore.ieee.org.

Digital Object Identifier 10.1109/JQE.2015.2425957

The principal advantage of OEOs comparatively to other oscillators is related to their very wide versatility in terms of time-scales. This time-scale versatility is possible owing to the fact that the system is built with optical and electronic devices, which feature significantly different and widely tunable bandwidth properties [5]–[8]. As a consequence, the nonlinear time-domain dynamics of OEOs can span over several orders of magnitude, and during the last three decades, research on various architectures of OEOs have demonstrated that they can be particularly far-reaching benchmarks for both fundamental and applied science [9].

From a fundamental point of view, optoelectronic oscillators have been used as experimental platforms for the investigation of the nonlinear dynamics of autonomous and/or delayed systems. In this regard, OEOs have for example permitted to understand some of the features related to the complexity of Ikeda-like delayed systems [9], [10]. From the standpoint of technological applications, OEOs can serve for the purpose of ultra-pure microwave generation [2]–[5], chaos cryptography [11], or neuromorphic computing [12].

When the bandwidth of the electric branch is narrow, the OEO essentially operates as a single-frequency oscillator. This configuration corresponds to a technological application of singular importance, namely ultra-stable radio-frequency (RF) generation. In this case, the system oscillates at the central frequency of an in-line narrowband RF filter whenever the overall loop gain is higher than the losses, following the well-known Barkhausen condition. From a nonlinear dynamics point of view, the oscillations originate from a primary Hopf bifurcation, with an oscillation frequency matching the resonance of the RF filter.

As it is known from the normal form theory of Hopf bifurcations, the amplitude of the oscillations is exponentially stable, while the phase is only neutrally stable. This neutral stability is a direct consequence of the phase invariance associated with limit-cycles oscillations, and is also at the origin of the phase drift responsible for phase noise in the stochastic regime. Along this line, coupled OEO architectures have been proven to allow for better phase noise performance, thereby indicating that the phase-locking of the auto-oscillator to another signal can lead to performance improvement under certain conditions that have to be determined.

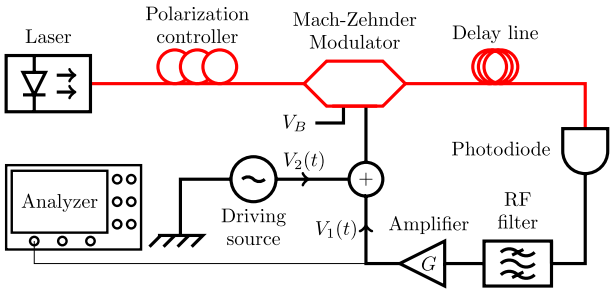

Fig. 1. Experimental setup of the OEO.

It is therefore of interest to investigate in detail the conditions under which such phase-locking occurs. The theory of phase-locking is intimately linked to the theory of phase-locked loops in system control, and to the theory of phase synchronization in nonlinear dynamics [14]. In the latter case, the genesis of phase synchronization can be traced back to the pioneering work of Christiaan Huygens on the synchronization of two pendulum clocks. Another milestone was achieved by Kuramoto [15], [16], who proposed a paradigmatic equation that allows to understand the ubiquitousness of phase synchronization in many areas [14], [20], [21]. Some of the technical methods used to study phase synchronization have been proposed by Arnold [17]–[23], which had demonstrated that phase-locking occurs in restricted areas of the parameter space which are nowadays referred to as "Arnold tongues".

In this paper, we perform a theoretical analysis that allows to understand the phase-locking behavior of single-loop optoelectronic oscillators when subjected to the influence of an external voltage source. We will investigate the conditions under which the driven oscillator will phase-lock to the external source. In particular, we are mainly interested by the influence of the frequency detuning between the driving and resonance frequencies on the phase-locking process.

The article is organized as follows. In Sec. II, we present the experimental set-up of the single-loop OEO. We also establish the equations ruling the dynamics of this system. In Sec. III, we focus on the case of null delay, and determine the fixed points of the oscillator, as well as their stability properties. We also describe analytically and numerically the phase-locking in terms of amplitude and frequency parameters of the driving source. We will also define the Arnold tongues region for weak and strong coupling. Section IV is devoted to the configuration where the delay is accounted for. The phase-locking phenomena are in this case analyzed using a delayed version of the Adler equation. The last section will conclude the article.

II. The Driven Optoelectronic Oscillator

The architecture of the single-loop OEO we are using is depicted in Fig. 1 [6], [7]. It consists of a continuous wave semiconductor laser of power P feeding a wideband electro-optic Mach-Zehnder modulator (MZM), characterized by a RF half-wave voltage $V_{\pi RF}$ and DC voltage $V_{\pi DC}$. The output of the MZM goes through an optical fiber which induces a time delay $T = 0.5\ \mu$s corresponding to 100 m of optical fiber. The delayed optical signal is detected by a fast photodiode with an optical/electrical conversion factor S. A narrow bandwidth filter with center frequency $\Omega_0/2\pi = 70$ MHz and a bandwidth $\Delta F = \Delta\Omega/2\pi = 10$ MHz is used to select the oscillation frequency of the OEO. A microwave amplifier with gain G amplifies the power of the electrical signal at the output of the filter. A frequency synthetizer is used as driving source, providing a stationary RF driving signal $V_2(t)$ whose frequency $F' = (\Omega_0 + \epsilon)/2\pi$ can be adjusted arbitrarily.

The coupled optoelectronic oscillator is equivalent to an electronic voltage controlled oscillator (VCO). The dynamics of the microwave oscillation can be therefore described in terms of a voltage $V(t)$ which is the sum of an external voltage $V_2(t)$ from the driving source and the voltage $V_1(t)$ from the amplifier output. The dynamics of the in-loop voltage can be described by the following integro-differential delay equation:

$$V_1(t) + \frac{1}{\Delta\Omega}\frac{dV_1(t)}{dt} + \frac{\Omega_0^2}{\Delta\Omega}\int_{t_0}^{t} V_1(s)ds = SGP\cos^2\left[\frac{\pi V_1(t-T)}{2V_{\pi RF}} + \frac{\pi V_2(t-T)}{2V_{\pi RF}} + \frac{\pi V_B}{2V_{\pi DC}}\right], \quad (1)$$

where the integro-differential term originates from the narrowband RF filtering, and the nonlinear term comes from the interference transfer function of the MZM [6], [7]. A simpler version of this equation would be based on the dimensionless voltages $x_i(t) = \pi V_i(t)/2V_{\pi RF}$ with $i = 1, 2$, and their delayed counterparts $x_{i,T}(t) \equiv x_i(t-T)$. The dimensionless equation therefore reads

$$x_1 + \frac{1}{\Delta\Omega}\frac{dx_1}{dt} + \frac{\Omega_0^2}{\Delta\Omega}\int_{t_0}^{t} x_1(s)ds = \beta\cos^2(x_{1,T} + x_{2,T} + \varphi), \quad (2)$$

where the constant parameters of the dimensionless Eq. (2) are the loop gain $\beta = \pi SGP/2V_{\pi RF}$ and the offset phase $\varphi = \pi V_B/2V_{\pi DC}$.

III. The Case OEO With Null Delay

In order to gain in depth understanding of the phase-locking mechanisms, it is useful to start our analysis with the case where the delay is set to zero.

Since the RF filter is narrowband, variable $x_1(t)$ can be expressed under the form of a quasi-sinusoidal signal with a slowly varying amplitude and frequency, while the driving signal is a sinusoidal signal with fixed amplitude and frequency. From a mathematical point of view, these dimensionless variables can be rewritten as:

$$x_1(t) = \frac{1}{2}\mathcal{A}(t)\,\mathrm{e}^{i\Omega_0 t} + \text{c.c.} \quad (3)$$

$$x_2(t) = \frac{1}{2}B\,\mathrm{e}^{i(\Omega_0+\epsilon)t} + \text{c.c.}, \quad (4)$$

where c.c. denotes the complex conjugate of the previous terms, ϵ is the detuning frequency shift parameter of the external signal, $\mathcal{A}(t) = A(t)e^{i\psi(t)}$ is the complex-valued slowly varying amplitude of the in-loop signal, and B is the fixed amplitude of the external signal. Note that B is

considered here as real-valued and positive (slowly-varying phase is null), without loss of generality.

Using Eqs. (3) and (4), the trigonometric formula $\cos^2 z = (1 + \cos 2z)/2$, and the Jacobi-Anger expansion given by

$$e^{iz\cos\xi} = J_0(z) + 2\sum_{n=1}^{+\infty} i^n J_n(z)\cos n\xi, \tag{5}$$

we can therefore rewrite Eq. (2) as

$$\dot{\mathcal{A}} = -\mu\mathcal{A} + 2\mu\gamma J_0[2B]J_{c1}[2|\mathcal{A}|]\mathcal{A} + 2\mu\gamma J_0[2|\mathcal{A}|]J_{c1}[2B]Be^{i\epsilon t}, \tag{6}$$

where $\gamma = \beta\sin 2\varphi$ is the effective loop gain, and $\mu = \Delta\Omega/2$ is the half-bandwidth [8], [13]. The function $J_{c1}(x) = J_1(x)/x$ denotes the first-order Bessel cardinal function. Equation (6) explicitly depends on time but we can remove this time dependence by introducing the variable transformation $\mathcal{Z} = \mathcal{A}e^{-i\epsilon t}$. As a result, we obtain the following equation:

$$\dot{\mathcal{Z}} = -\mu\mathcal{Z} - i\epsilon\mathcal{Z} + 2\mu\gamma J_0[2B]J_{c1}[2|\mathcal{Z}|]\mathcal{Z} + 2\mu\gamma J_0[2|\mathcal{Z}|]J_{c1}[2B]B, \tag{7}$$

where

$$\mathcal{Z} = Ze^{i\phi(t)} \text{ with } \phi(t) = \psi(t) - \epsilon t. \tag{8}$$

is the new dynamical variable.

A. Determination of Fixed Points and Their Stability

In this section we determine the steady state amplitude $\mathcal{Z}_{st}$ of the central mode by using the relationships $\dot{\mathcal{Z}} = 0$ and $|\mathcal{Z}_{st}| = |\mathcal{A}_{st}|$. We rescale the detuning frequency ϵ to a dimensionless parameter ε following $\varepsilon = \epsilon/\mu$. Hence, the steady state equation obeys the following equation:

$$\varepsilon^2 Z_{st}^2 + Z_{st}^2\{1 - 2\gamma J_0[2B]J_{c1}[2Z_{st}]\}^2 - 4\gamma^2\{J_0[2Z_{st}]J_{c1}[2B])B\}^2 = 0. \tag{9}$$

This nonlinear algebraic equation depends on the amplitude and the detuning frequency of the driving source. The steady state can not be analytically evaluated, and numerical simulation is needed to understand how the in-loop oscillation amplitude is influenced by the driving signal. We first study the effect of driving amplitude B at $\varepsilon = 0$, and then we study the contribution of the frequency detuning. A trivial solution of this equation $Z_{st} = 0$ is obtained whenever the amplitude B or the gain γ is null, regardless of the value of the detuning ε. For the case of the non-driven oscillator ($B = 0$), it is well known that there are two fixed points: the trivial fixed point $Z_0 = 0$ and the non-trivial solution obeying $2\gamma J_{c1}[2|Z_{osc}|] = 1$, which exists only when $|\gamma| > 1$ [8]. The critical value $|\gamma_{cr}| = 1$ corresponds to a Hopf bifurcation leading to single tone oscillations: the trivial fixed point $Z_0 = 0$ is stable for $\gamma < 1$, but looses its stability for $\gamma > 1$ in favor of the non-trivial solution Z_{osc}.

When the detuning ε is null, the steady-state equation becomes a function of the amplitude of external source. This case is described by the following equation:

$$Z_{st} - \gamma J_0[2B]J_1[2Z_{st}] \pm \gamma J_0[2Z_{st}]J_1[2B] = 0. \tag{10}$$

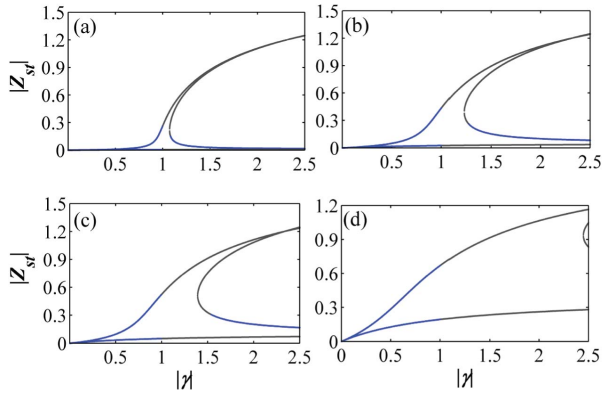

Fig. 2. Numerical evaluation of the fixed point Z_{st} at different values of B when $\varepsilon = 0$, using Eq. (10). (a) $B = 0.01$, (b) $B = 0.05$, (c) $B = 0.1$, and (d) $B = 0.4$. The solid blue line characterizes stable fixed points and the solid grey line represents unstable fixed points.

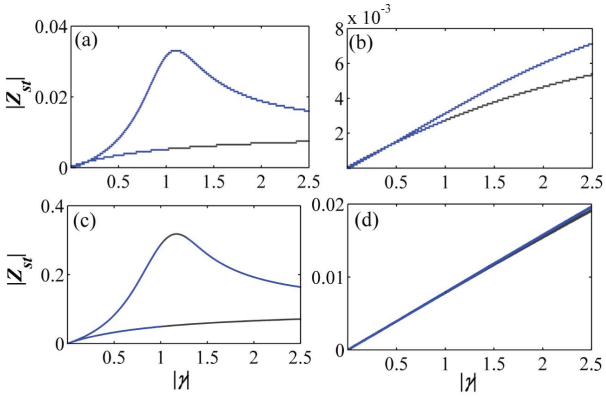

Fig. 3. Numerical evaluation of the fixed point Z_{st} at different values of the detuning ε using Eq. (9). (a) $B = 0.01$ and $\varepsilon = 0.01$; (b) $B = 0.01$ and $\varepsilon = 0.1$; (c) $B = 0.1$ and $\varepsilon = 0.01$; (d) $B = 0.1$ and $\varepsilon = 0.3$. The solid blue line characterizes stable fixed points and the solid gray line represents unstable fixed point.

We can numerically determine the fixed point at different value of driving amplitude B. In Fig. 2 we plot for different values of B the fixed point at $\varepsilon = 0$. Figure 3 gives the evolution for different values of the detuning ε when it is not null., and it is seen that for a small detuning frequency restricted to the bandwidth of the RF filter, there is noticeable variation of the threshold. It can be observed in Figs. 2 and 3 that there can be multiple solutions for the same value of the gain. That multistability is induced by the presence of the forcing signal B in the Eq. (10). The oscillations that are actually observable correspond to stable fixed points (depicted in blue in the figures).

We now determine the stability properties of the fixed points. We have to note that the fixed points are not explicitly defined for $\gamma \neq 0$. In order to study their stability, we have to perturb Eq. (8) and check if the perturbation grows or decreases depending on the driving source parameters and the normalized value of the normalized gain. Using the following relation

$$|\mathcal{Z}_{st} + \delta\mathcal{Z}| = Z_{st} + \frac{1}{2}\delta\mathcal{Z} + \frac{1}{2}\delta\mathcal{Z}^*, \tag{11}$$

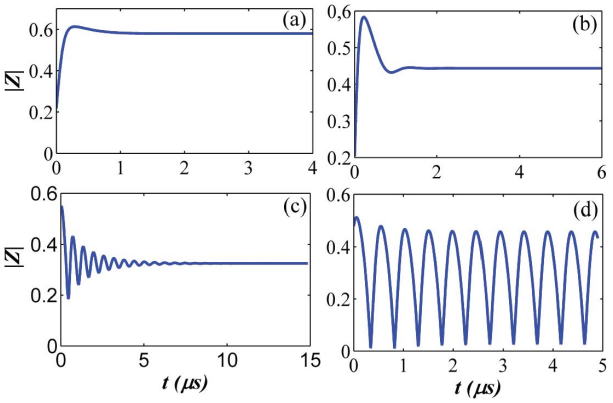

Fig. 4. Numerical simulation of Eq. (7) for various detuning frequency values, with $B = 0.1$ and $\gamma = 1.1$. The initial condition has been uniformly set at $\mathcal{Z} = 0.2$. (a) $\varepsilon = 0.1$; (b) $\varepsilon = 0.2$; (c) $\varepsilon = 0.3$; (d) $\varepsilon = 0.4$.

where the star symbol (*) denotes the complex conjugate, we obtain the autonomous perturbation flow

$$\delta\dot{\mathcal{Z}} = k\delta\mathcal{Z} + \alpha\delta\mathcal{Z}^*$$
$$\delta\dot{\mathcal{Z}}^* = \alpha\delta\mathcal{Z} + k^*\delta\mathcal{Z}^* \tag{12}$$

where the parameters k (complex-valued) and α (real-valued) are defined as:

$$k = -\mu - 2\mu\gamma\,\mathrm{J}_0[2B]\mathrm{J}_{c1}[2Z_{\mathrm{st}}] + 2\mu\gamma\,\mathrm{J}_0[2|Z_{\mathrm{st}}|]\mathrm{J}_0[2B] - 4\mu\gamma\,\mathrm{J}_{c1}[2B]\mathrm{J}_1[2|Z_{\mathrm{st}}|]B - i\epsilon, \tag{13}$$

$$\alpha = 2\mu\gamma\,\mathrm{J}_0[2B]\mathrm{J}_0[2Z_{\mathrm{st}}] - 4\mu\gamma\,\mathrm{J}_0[2B]\mathrm{J}_{c1}[2Z_{\mathrm{st}}] - 2\mu\gamma\,\mathrm{J}_1[2B]\mathrm{J}_1[2Z_{\mathrm{st}}]. \tag{14}$$

The characteristic equation for the eigenvalues is given by

$$\lambda^2 - (k + k^*)\lambda + (kk^* - \alpha^2) = 0, \tag{15}$$

with solutions

$$\lambda_{1,2} = \Re(k) \pm \sqrt{\alpha^2 - \varepsilon^2}. \tag{16}$$

The sign of these eigenvalues defines if the fixed point is stable or not. If $|\alpha| < \varepsilon$, both eigenvalues are complex and the fixed point is asymptotically stable if all real parts are negative. In that case, Eq. (16) should be rewritten as:

$$\lambda_{1,2} = \Re(k) \pm i\sqrt{\varepsilon^2 - \alpha^2}. \tag{17}$$

These two eigenvalues are complex conjugate in the presence of the detuning frequency and have the negative real part described by the blue line in Fig. 3. This corresponds to an asymptotical stability for this fixed point. For the case with $\varepsilon = 0$ presented in Fig. 2, both eigenvalues are real and have real parts with opposite signs. An important observation is that for all values of B and ε, the fixed point changes its stability at $\gamma = 1$. In Fig. 4, we illustrate the numerical simulation of Eq. (7) for four values of the detuning frequency ε. It can be seen that the amplitude converges to the stable fixed point for $\varepsilon = 0.1$, 0.2 and 0.3, but leads to oscillations for $\varepsilon = 0.4$.

From a more global perspective, the oscillations in OEOs arise through the scenario presented in Fig. 5, which is the 3D-display of an experimental bifurcation diagram obtained in absence of the driving source. Below a critical value, the trivial fixed point is stable, while above this value, a limit-cycle induced by a Hopf bifurcations emerges, thereby leading to self-sustained, single-tone oscillations. When the driving force is set on, we typically obtain the dynamics displayed in Fig. 6, which is the experimental plot for the in-loop oscillation for $\gamma = 1.1$ corresponding to a laser injection current of 32.4 mA, The amplitude of external source is normalized at $B = 0.1$ and the detuning frequency is normalized at $\varepsilon = 0.4$. Figure 6 is in concordance with the numerical time trace displayed in Fig. 4d.

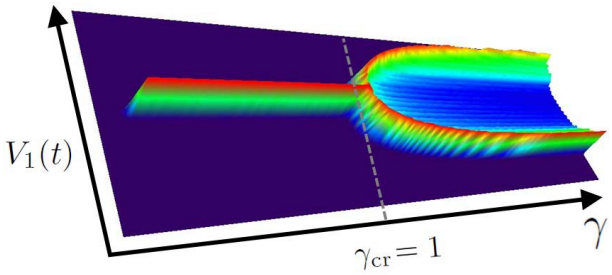

Fig. 5. 3D-Display of an experimental bifurcation diagram obtained when the system is not driven ($B = 0$). The height is a probability density distribution, and the gain γ is varied from 0 to 3 (laser current varied from 0 to 70 mA). The color code is such that red (blue) indicates high (low) probability. When the gain is smaller than 1, the trivial fixed point is stable. Beyond that critical value (Hopf bifucation point), stable oscillations are triggered.

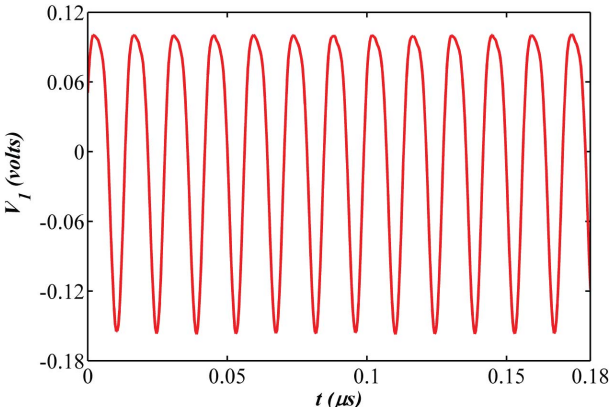

Fig. 6. Experimental plot of the in-loop oscillations. The normalised gain is $\gamma = 1.1$, corresponding to a laser injection current of 32.4 mA. This timetrace is to be compared with the one of Fig. 4(d).

B. The Phase Equation

In this section, we investigate in detail the problem of phase-locking between the external and in-loop signals. For this purpose, we define the phase equation using Eqs. (7) and (8), following

$$\frac{d\phi}{dt} = -\varepsilon + \eta\sin\phi, \tag{18}$$

where $\eta = -2\gamma\,\mathrm{J}_0[2Z]\mathrm{J}_{c1}[2B]B/Z$. This equation for the phase is sometimes referred to as the Adler equation [14], [18]. We assume that in the absence of interaction ($B = 0$), the phase ψ of this optoelectronic oscillator is constant [8]. The important task here is to determine the stability of the phase difference and study the case where we observe a phase-locked regime. We can see

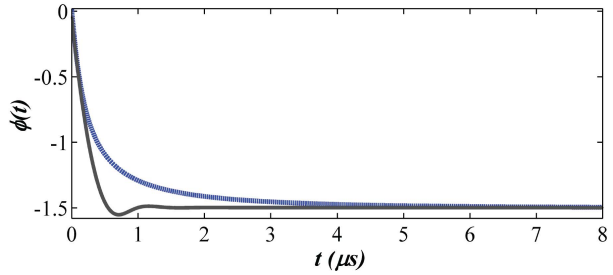

Fig. 7. Variations of the phase difference ϕ. The blue line represents the results from the numerical simulation using Eq. (18) with $\varepsilon(\mu) = 0.2$, $B = 0.1$, $\gamma = 1.1$, $Z_{\text{st}} = 0.44$, and the gray line represents the results from numerical simulation using Eq. (7) with $\varepsilon(\mu) = 0.2$, $B = 0.1$, $\gamma = 1.1$.

that from Eq. (18), the oscillator can be locked with an external source, exhibiting a wide variety of Arnold tongues obtained as a function of the different values of normalized external voltage.

The stability of phase equation (18) is studied by the determination of the fixed point of this equation through $\dot{\phi} = 0$ yields

$$\sin\phi = \frac{\varepsilon}{\eta}. \tag{19}$$

Three particular cases can therefore be observed depending on the magnitude of the ratio ε/η.

The first case is $\varepsilon = 0$, corresponding to the case where x_1 and x_2 have the same frequency. Here, the fixed point $\phi_{\text{st}} = 0$ is stable, and we have $\phi_{\text{st}} = \psi_{\text{st}} = 0$.

The second case is $|\varepsilon/\eta| < 1$, and here, the system should have two fixed points, with one being stable and the other unstable. We observe phase-locking and the constant phase difference can be expressed as

$$\phi_{\text{st}} = \arcsin\frac{\varepsilon}{\eta}. \tag{20}$$

In Fig. 7, we represent the time evolution of the phase difference for $\varepsilon = 0.01$ and for $\varepsilon = 0.4$. The gray line is the numerical simulation using Eq. (7) and the blue line represents the numerical simulation using equation (18) when Z_{st} is constant. These curves explain that when the condition $|\varepsilon/\eta| < 1$ is satisfied, the phase difference evolves towards stable oscillations.

According to Eq. (20), we define the steady state solution of the OEO. We remark that for a weak coupling, the phase difference is slowly attracted to the fixed point and for the strong coupling there is a rapid attraction. The instantaneous phase $\psi_{\text{st}} = \phi_{\text{st}} + \varepsilon t$ of the oscillator depends on the phase of the driving source, and this equation describes a mode-locking behavior of the envelope which oscillates at the frequency of driving source ε. In order to study the stability of the fixed point, we have to perturb it and check if the perturbation grows or decreases depending on the frequency shift ε. By neglecting the high order nonlinear terms, the perturbation equation for $\delta\phi$ is

$$\delta\dot{\phi} = \lambda_p\,\delta\phi, \tag{21}$$

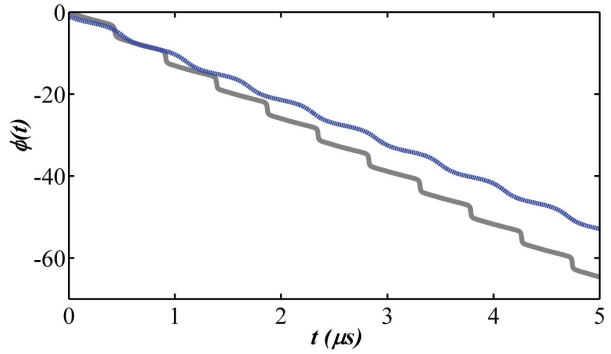

Fig. 8. Variations of the phase difference ϕ. The blue line represents the numerical simulation using Eq. (7) with $\varepsilon = 0.4$, $B = 0.1$, $\gamma = 1.1$, and the gray line represents the numerical simulation using Eq. (18) with $\varepsilon = 0.4$, $B = 0.1$, $\gamma = 1.1$, $Z_{\text{st}} = 0.41$.

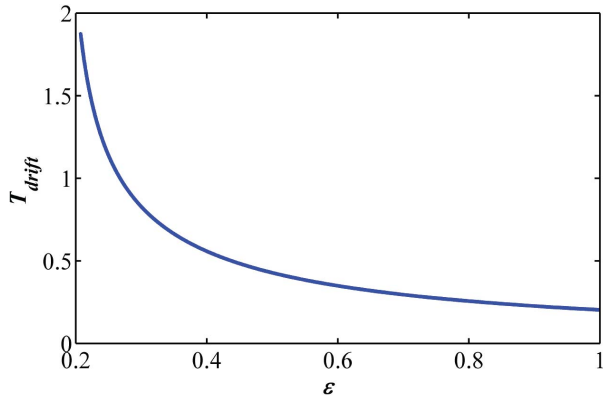

Fig. 9. Variation of the period drift using Eq. (23) with $B = 0.1$, $\gamma = 1.1$ and η is calculated using Eq. (7) in therm of Z.

where

$$\lambda_p = \eta\,\cos\left[\arcsin\frac{\varepsilon}{\eta}\right] = \pm\sqrt{\eta^2 - \varepsilon^2}. \tag{22}$$

The exponential growth rate λ is here positive or negative since the condition $|\varepsilon/\eta| < 1$ is satisfied. It can be assumed here that the phase difference is asymptotically stable for the case where the exponential rate $\lambda < 0$. This is a direct indicator of phase synchronization in our OEO .

The last case corresponds to $|\varepsilon/\eta| > 1$. Here, both fixed points disappear and the phase-locking is irremediably lost. The phase difference diverges because of the deterministic phase drift [20]. The phase difference increases slowly in the form of a sine wave and the period of the phase-drift can be evaluated as [16].

$$T_{\text{drift}} = \frac{2\pi}{\sqrt{\varepsilon^2 - \eta^2}}. \tag{23}$$

The numerical simulation of phase equation for the case of phase drift is shown in Fig. 8. We observe in this figure that the phase difference is unstable, thereby characterizing the phase-drift. The analytical calculation of the period of the drift using Eq. (23) gives $T_{\text{drift}} = 0.481$ and the evaluation in Fig. 9 shows $T_{\text{drift}} = 0.468$. Figure 9 explains the variation of the period of the drift as a function of detuning frequency.

IV. Influence of the Delay

The time-delay induces an infinite-dimensionality in the system, and when combined with the inherent nonlinearity of the system, it leads to significantly more complex dynamical behaviors. When the delay is accounted for, the slowly-varying amplitude of the microwave obeys

$$\dot{\mathcal{A}} = -\mu\mathcal{A} - 2\mu\gamma\, \mathrm{e}^{-\mathrm{i}\Omega_0\mathrm{T}}\mathrm{J}_0[2B]\mathrm{J}_{c1}[2A_T]\mathcal{A}_T - 2\mu\gamma\, \mathrm{e}^{-\mathrm{i}\Omega_0\mathrm{T}}\mathrm{J}_0[2A_T]\mathrm{J}_{c1}[2B]B\mathrm{e}^{i\epsilon(t-T)}, \quad (24)$$

where the parameters are identical to those of Eq. (6). The delay-induced phase-shift term $\mathrm{e}^{-i\Omega_0 T}$ can be set to -1 [8], and the explicit dependence in Eq. (24) can be removed by introducing the variable transformation $\mathcal{G} = \mathcal{A}\mathrm{e}^{-i\epsilon t}$, thereby leading to the delayed-differential equation

$$\dot{\mathcal{G}} = -\mu\mathcal{G} - i\epsilon\mathcal{G} + 2\mu\gamma\,\mathrm{J}_0[2B]\mathrm{J}_{c1}[2G_T]\mathcal{G}_T\mathrm{e}^{-i\epsilon T} + 2\mu\gamma\,\mathrm{J}_0[2G_T]\mathrm{J}_{c1}[2B]B\mathrm{e}^{-i\epsilon T}. \quad (25)$$

In this equation we observe that the microwave envelope is perturbed by the amplitude and detuning frequency of the driving oscillator. In the next sub-section we study their effect on the dynamics of the optoelectronic oscillator.

A. Amplitude and Phase Dynamics

The stationary solutions obey the nonlinear algebraic equation depending on the the fixed point amplitude G_{st} following

$$(1 + i\varepsilon)G_{\mathrm{st}} - (\rho_1\mathrm{J}_1[2|G_{\mathrm{st}}|] + \rho_0\mathrm{J}_0[2|G_{\mathrm{st}}|])\mathrm{e}^{-i\epsilon T} = 0, \quad (26)$$

where $\rho_0 = \gamma\,\mathrm{J}_0[2B]$, $\rho_1 = \gamma\,\mathrm{J}_1[2B]$ and $\varepsilon = \epsilon/\mu$. This equation is solved by considering the real and imaginary parts separately. We arrive in the system described as

$$G_{\mathrm{st}} - (\rho_0\mathrm{J}_1[2|G_{\mathrm{st}}|] + \rho_1\mathrm{J}_0[2|G_{\mathrm{st}}|])\cos\epsilon T = 0 \quad (27)$$

$$\varepsilon G_{\mathrm{st}} - (\rho_0\mathrm{J}_1[2|G_{\mathrm{st}}|] + \rho_1\mathrm{J}_0[2|G_{\mathrm{st}}|])\sin\epsilon T = 0. \quad (28)$$

When the gain exceeds a given threshold value, the fixed points loose their stability and a complex time-domain dynamics is triggered.

B. Phase Dynamics

The phase dynamics of the system can be analyzed after introducing new real variables G and ϕ following

$$\mathcal{G} = G\mathrm{e}^{i\phi(t)}, \quad (29)$$

where $G \geq 0$ and $\phi = \psi(t) - \epsilon t$ stand for the microwave amplitude and phase difference between the two oscillators. Substituting this representation into the Eq. (25) yields two equations for the amplitude and the phase difference:

$$\dot{G} = -\mu G + 2\mu\gamma\,\mathrm{J}_0[2B]\mathrm{J}_{c1}[2G_T]G_T \times\cos(\phi_T - \phi - \epsilon T) + 2\mu\gamma\,B\mathrm{J}_{c1}[2B]\mathrm{J}_0[2G_T]\cos(\phi + \epsilon T), \quad (30)$$

$$\dot{\phi} = -\epsilon + 2\mu\gamma\,\mathrm{J}_0[2B]\mathrm{J}_{c1}[2G_T]G_T \times\sin(\phi_T - \phi - \epsilon T) - 2\mu\gamma\,B\mathrm{J}_{c1}[2B]\mathrm{J}_0[2G_T]\sin(\phi + \epsilon T). \quad (31)$$

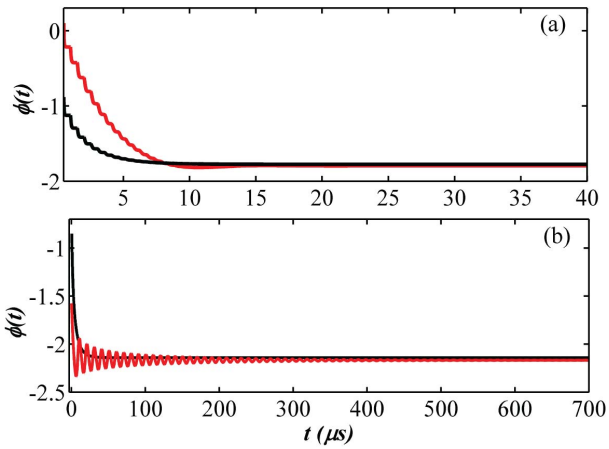

Fig. 10. Time variation of the phase difference with $B = 0.2$ and $\epsilon = 0.5$ MHz, $T = 0.5$ μs and for (a) $\gamma = 1.3$ and (b) $\gamma = 1.43$. The solid red line displays the the results of the phase equation given in Eq. (25) while the solid black line displays the analytical phase equation given in Eq. (32) for the same values of normalized gain.

This set of equations can be further simplified, and lead to the phase difference equation:

$$\dot{\phi} = -\Delta - K\sin\phi + \eta\sin(\phi_T - \phi). \quad (32)$$

where the parameters Δ, η and K are respectively defined as follows:

$$\Delta = \epsilon + \mu\tan\epsilon T \quad (33)$$

$$\eta = \frac{2\mu\gamma\,\mathrm{J}_0[2B]\mathrm{J}_{c1}[2G_T]G_T}{G\cos\epsilon T} \quad (34)$$

$$K = \frac{2\mu\gamma\,B\mathrm{J}_{c1}[2B]\mathrm{J}_0[2G_T]}{G\cos\epsilon T}. \quad (35)$$

Equation (32) is the delayed phase equation that will describe the phase-locking effects of interest in our system. In the literature, this equation is known as the delayed Adler equation when the parameters are constant. This case is studied in ref. [24] and the synchronization region is explicitly described within the framework of Arnold Tongues theory.

C. Stability and Phase Synchronization of the System

The stability of Eq. (32) can be studied by determining the fixed points of the phase equation. We therefore set $\dot{\phi} = 0$, leading to $K\sin\phi = -\Delta$. Three particular cases have to be analyzed in detail.

- *Case* $|\Delta/K| = 0$*:* we are led to $\Delta = 0$, that is, $\epsilon + \mu\tan\epsilon T = 0$ or $\epsilon = 0$. In this case, we have one fixed point and the coupled OEO oscillates with the central frequency Ω_0. This is a trivial case of in-phase synchronization.
- *Case* $|\Delta/K| > 1$*:* here, there is no fixed point and the phase difference diverges. This case also encompasses the regime where the system can display a chaotic behavior.
- *Case* $|\Delta/K| < 1$*:* there are two fixed points defined by

$$\phi_{\mathrm{st}} = -\arcsin\frac{\Delta}{K}, \quad (36)$$

with one being stable (corresponding to phase-locking) and the other being unstable. The stability of the phase-looked solution

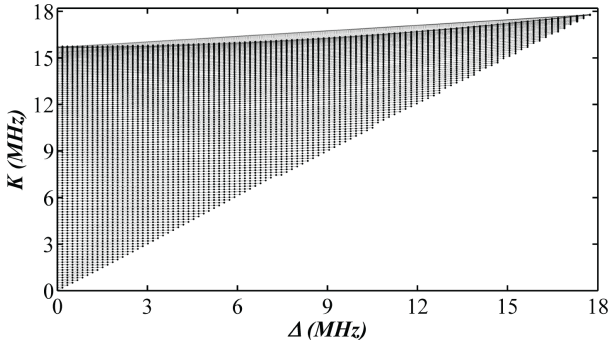

Fig. 11. Numerical simulation of phase-locked solution for $\gamma = 0.5$. The shaded area corresponds to the phase-locked states.

is determined by the root of the corresponding characteristic equation

$$\lambda - \eta e^{-\lambda T} + \eta + \sqrt{K^2 - \Delta^2} = 0. \tag{37}$$

where λ is the complex eigenvalue. Using the fact that λT is small, we use the a Taylor expansion of exponential term $e^{-\lambda T} \simeq 1 - \lambda T$ to determine the following approximation of the eigenvalue:

$$\lambda \simeq -\frac{\eta + \sqrt{K^2 - \eta^2}}{1 + \eta T}. \tag{38}$$

When $\lambda < 0$, the dynamics of the phase difference in the system is asymptotically stable, as it can be observed in Fig. 10. In that case, all the trajectories of the phase converge to the stable value and the OEO becomes phase-locked to the external driving. Figure 11 shows the area in the parameter space $\Delta - K$ where phase-locking occurs. This figure is obtained by varying the driving voltage B from 0 to 1 at constant gain $\gamma = 0.5$. For the natural frequency Δ inside the shaded area (Arnold tongue), the voltage controlled oscillator entrained the optoelectronic oscillator to a synchronous state.

V. Conclusion

In this article, we have analyzed the phase synchronization of an optoelectronic oscillator coupled to an external source. The global system was therefore similar to a voltage controlled oscillator. We have proposed an analytical model that enabled us to investigate the behavior of the phase difference between the OEO and the driving source. We have then defined the regimes of weak and strong coupling on the base of our stability analysis. It appeared that for given values of the external driving amplitude and frequency, there exists a phase-locking regime where synchronization occurs. The OEO is therefore a system where an external source can be used to phase-lock its frequency. Further research will be performed in order to study the efficiency of phase-locking in various architectures of particular technological interest.

References

[1] A. Neyer and E. Voges, "Dynamics of electrooptic bistable devices with delayed feedback," *IEEE J. Quantum Electron.*, vol. QE-18, no. 12, pp. 2009–2015, Dec. 1982.

[2] X. S. Yao and L. Maleki, "High frequency optical subcarrier generator," *Electron. Lett.*, vol. 30, no. 18, pp. 1525–1526, 1994.

[3] X. S. Yao and L. Maleki, "Optoelectronic microwave oscillator," *J. Opt. Soc. Amer. B*, vol. 13, no. 8, pp. 1725–1735, 1996.

[4] S. Poinsot, H. Porte, J.-P. Goedgebuer, W. T. Rhodes, and B. Boussert, "Continuous radio-frequency tuning of an optoelectronic oscillator with dispersive feedback," *Opt. Lett.*, vol. 27, no. 15, pp. 1300–1302, 2002.

[5] L. Maleki, "Sources: The optoelectronic oscillator," *Nature Photon.*, vol. 5, no. 12, pp. 728–730, Dec. 2011.

[6] Y. K. Chembo, L. Larger, H. Tavernier, R. Bendoula, E. Rubiola, and P. Colet, "Dynamic instabilities of microwaves generated with optoelectronic oscillators," *Opt. Lett.*, vol. 32, no. 17, pp. 2571–2573, 2007.

[7] Y. K. Chembo, L. Larger, R. Bendoula, and P. Colet, "Effects of gain and bandwidth on the multimode behavior of optoelectronic microwave oscillators," *Opt. Exp.*, vol. 16, no. 12, pp. 9067–9072, 2008.

[8] Y. K. Chembo, L. Larger, and P. Colet, "Nonlinear dynamics and spectral stability of optoelectronic microwave oscillators," *IEEE J. Quantum Electron.*, vol. 44, no. 9, pp. 858–866, Sep. 2008.

[9] L. Larger, "Complexity in electro-optic delay dynamics: Modelling, design and applications," *Philos. Trans. Roy. Soc. A, Math., Phys., Eng. Sci.*, vol. 371, no. 1999, p. 20120464, 2013.

[10] Y. C. Kouomou, P. Colet, L. Larger, and N. Gastaud, "Chaotic breathers in delayed electro-optical systems," *Phys. Rev. Lett.*, vol. 95, p. 203903, Nov. 2005.

[11] A. Argyris *et al.*, "Chaos-based communications at high bit rates using commercial fibre-optic links," *Nature*, vol. 438, pp. 343–346, Sep. 2005.

[12] R. Martinenghi, S. Rybalko, M. Jacquot, Y. K. Chembo, and L. Larger, "Photonic nonlinear transient computing with multiple-delay wavelength dynamics," *Phys. Rev. Lett.*, vol. 108, p. 244101, Jun. 2012.

[13] R. M. Nguimdo, R. Lavrov, P. Colet, M. Jacquot, Y. K. Chembo, and L. Larger, "Effect of fiber dispersion on broadband chaos communications implemented by electro-optic nonlinear delay phase dynamics," *J. Lightw. Technol.*, vol. 28, no. 18, pp. 2688–2696, Sep. 15, 2010.

[14] A. S. Pikovsky, M. G. Rosenblum, M. A. Zaks, and J. Kurths, "Phase synchronization of regular and chaotic oscillators," in *Handbook of Chaos Control*, H. G. Schuster, Ed. New York, NY, USA: Wiley, 1999, pp. 305–328.

[15] K. Trojanowski and L. Longa, "Synchronization of Kuramoto oscillators with distance-dependent delay," *Acta Phys. Polonica B*, vol. 44, no. 5, pp. 991–995, 2013.

[16] A. A. Koronovskii, M. K. Kurovskaya, O. I. Moskalenko, and A. E. Hramov, "Two scenarios of breaking chaotic phase synchronization," *Tech. Phys.*, vol. 52, no. 1, pp. 19–26, 2006.

[17] S. Boccaletti, J. Kurths, G. Osipov, D. L. Valladares, and C. S. Zhou, "The synchronization of chaotic systems," *Phys. Rep.*, vol. 366, nos. 1–2, pp. 1–101, 2002.

[18] M. G. Rosenblum, A. S. Pikovsky, and J. Kurths, "Phase synchronization of chaotic oscillators," *Phys. Rev. Lett.*, vol. 76, pp. 1804–1807, Mar. 1996.

[19] M. G. Rosenblum, A. S. Pikovsky, and J. Kurths, "From phase to lag synchronization in coupled chaotic oscillators," *Phys. Rev. Lett.*, vol. 78, pp. 4193–4196, Jun. 1997.

[20] S. H. Strogatz, *Nonlinear Dynamics And Chaos*. New York, NY, USA: Addison-Wesley, 1994.

[21] M. G. Earl and S. H. Strogatz, "Synchronization in oscillator networks with delayed coupling: A stability criterion," *Phys. Rev. E*, vol. 63, pp. 036204-1–036204-4, Mar. 2003.

[22] R. V. Jensen, "Synchronization of driven nonlinear oscillators," *Amer. J. Phys.*, vol. 70, no. 6, pp. 607–619, 2002.

[23] D. García-Álvarez, A. Stefanovska, and P. V. E. McClintock, "High-order synchronization, transitions, and competition among Arnold tongues in a rotator under harmonic forcing," *Phys. Rev. E*, vol. 77, p. 056203, May 2008.

[24] Y. N. Kyrychko, K. B. Blyuss, and E. Schöll, "Amplitude and phase dynamics in oscillators with distributed-delay coupling," *Philos. Trans. Roy. Soc. A, Math., Phys., Eng. Sci.*, vol. 371, pp. 20120466-1–20120466-22, Aug. 2013.

[25] Y. K. Chembo, A. Hmima, P.-A. Lacourt, L. Larger, and J. M. Dudley, "Generation of ultralow jitter optical pulses using optoelectronic oscillators with time-lens soliton-assisted compression," *J. Lightw. Technol.*, vol. 27, no. 22, pp. 5160–5167, Nov. 15, 2009.

Alain Francis Talla received the M.S. degree in physics from the University of Yaoundé I, Cameroon, in 2011, where he is currently pursuing the Ph.D. degree with a focus on nonlinear and stochastic dynamics of optoelectronic oscillators with intermediate frequencies.

Romain Martinenghi received the Ph.D. degree with a focus on photonic reservoir computing from the Franche Comté Electronique Mécanique Thermique et Optique—Sciences et Technologies (FEMTO-ST) Institute, Besançon, France, in 2012. He is currently with the FEMTO-ST Institute as a Post-Doctoral Research Fellow on the stabilization of high spectral purity microwave sources.

Géraud R. Goune Chengui received the M.S. degree in physics from the University of Dschang, Cameroon, in 2010. He is currently pursuing the Ph.D. degree with the University of Yaoundé I, Cameroon, with a focus on multiscale nonlinear dynamics of optoelectronic oscillators.

Jimmi H. Talla Mbé received the Ph.D. degree from the University of Yaoundé I, Cameroon, in 2012. He was a Post-Doctoral Fellow with the Franche Comté Electronique Mécanique Thermique et Optique—Sciences et Technologies Institute, Besançon, France, in 2012. He is currently a Post-Doctoral Fellow with the Laboratory of Modeling and Simulation in Engineering, Biomimetics and Prototypes, University of Yaoundé I. His research interests include nonlinear dynamics, optoelectronics, optomechanics, and optical metrology.

Khaldoun Saleh received the Ph.D. degree in microwaves, electromagnetism, and optoelectronics from Toulouse III University, France, in 2012. He is currently with the Franche Comté Electronique Mécanique Thermique et Optique—Sciences et Technologies Institute, Besançon, France, as a Post-Doctoral Research Fellow, works on the improvement of high spectral purity microwave sources based on optical whispering gallery mode resonators.

Aurélien Coillet received the Ph.D. degree from the University of Burgundy, Dijon, France, in 2011. From 2012 to 2014, he was a Post-Doctoral Fellow with the Franche Comté Electronique Mécanique Thermique et Optique—Sciences et Technologies Institute, Besançon, France. He is currently with the National Institute of Standards and Technology, Boulder, CO, USA. His research interests include ultrahigh-Q whispering-gallery mode resonators, optoelectronics, nonlinear optics, and nonlinear dynamics.

Guoping Lin received the Ph.D. degrees in optics and physics from Xiamen University, China, and the École Normale Supérieure, Paris, France, in 2010. From 2011 to 2013, he was a National Aeronautics and Space Administration Post-Doctoral Program Fellow with the Jet Propulsion Laboratory, Pasadena, USA. He is currently a Post-Doctoral Fellow with the Franche Comté Electronique Mécanique Thermique et Optique—Sciences et Technologies Institute, Besançon, France, where he is working on miniature spectrally pure microwave sources based on ultrahigh-Q crystalline optical resonators.

Paul Woafo received the Ph.D. degree in physics from the University of Yaoundé I, in 1992, and the Doctorat d'Etat degree in physics in 1997. He is currently a Full Professor with the University of Yaoundé I, and the Head of the Laboratory of Modeling and Simulation in Engineering, Biomimetics and Prototypes. He is a Senior Associate with the International Center for Theoretical Physics, and a Georg Forster Fellow of the Humboldt Foundation, Germany. He has authored over 160 refereed articles in international journals. His research interests involve the nonlinear and stochastic dynamics in optoelectronics, electromechanics, and biological systems. He was a member of the International Union of Pure and Applied Physics Commission for Statistical Physics. He received the TWAS Prize for Young Scientists in 2004. He is a Founding Member and was the President of the Cameroonian Physical Society, and the Vice President of the African Physical Society.

Yanne K. Chembo (SM'12) received the Ph.D. degree in physics from the University of Yaoundé I, in 2005, and the Ph.D. degree in laser physics from the Institute for Cross-Disciplinary Physics and Complex Systems, Palma de Mallorca, Spain, in 2006. In 2007 and 2008, he was a Post-Doctoral Fellow with the Franche Comté Electronique Mécanique Thermique et Optique—Sciences et Technologies (FEMTO-ST) Institute, Besançon, France. In 2009, he was a National Aeronautics and Space Administration Post-Doctoral Program Fellow with the Jet Propulsion Laboratory, Pasadena, USA. Since 2010, he has been a Senior Research Scientist with the Centre National de la Recherche Scientifique, FEMTO-ST Institute. He has authored over 100 articles in international journals and conference proceedings. His research interests involve microwave photonics, optoelectronics, complex systems, applied nonlinear, stochastic and quantum dynamics.